JIRBDAI

Journal of Institutional Research, Big Data Analytics and Innovation

Spectral Numerical Study of Internal Heat Generating Magneto-Convective Fluid Flow Through Poro-Elastic Media

F. T. Osho [1, 2], O. Olowogunle [3], A. D. Adebayo[4]

[1]Department of Mathematics, Adeyemi Federal University of Education, Ondo State, Nigeria.
[2]Department of Mathematics and Statistics, Redeemer's University, Ede, Nigeria,
[3.4] Department of Kinetic Education. Adeyemi Federal University of Education, Ondo State, Nigeria.
[1]oshoft@afued.edu.ng, [2]olowogunleo@run.edu.ng, [3]adebayoayodele54@gmail.com

ABSTRACT: The paper examines the uniqueness of the spectral quasi-linearization solution to the coupled system that models the steady flow and heat transfer of a radiative hydro-magnetic Jeffery fluid in a poro-elastic medium through a vertical channel. The dimensionless coupled boundary value problem is solved using the shooting-Runge-Kutta method and validated with the Spectral Chebyshev Collocation Method. The study formulates a coupled system of nonlinear boundary value problems that govern the solid displacement, fluid velocity, and temperature fields. Existence and uniqueness of solutions are theoretically established using Lipschitz continuity arguments. Numerical and graphical results demonstrate strong agreement across solution techniques, confirming the uniqueness and convergence of the solutions. The two results were compared with the previous result obtained in the literature. Numerical comparison of the results features well in this work, establishing the uniqueness of the solutions. Parametric analysis reveals that porous permeability, thermal radiation, magnetic field strength (Hartmann number), and kinetic heat generation significantly influence displacement, velocity, and temperature distributions within the channel, thereby highlighting the complex interplay between magnetic, thermal, and poroelastic effects in non-Newtonian fluid flow systems.

KEYWORDS: convective flow, Viscoelastic fluids, poro-elastic medium.

I. INTRODUCTION

Disciplines such as biological, chemical, and environmental engineering, among others, have a great interest in convective flow through porous channels. It has enhanced thermal performance, mass transfer, and heat transfer, and is also a crucial component of fluid mechanics. Sreepada and Onbela [1] investigated the convective flow of Casson fluids in a non-Darcy porous medium with convective boundary conditions. They discovered that increased heat transfer significantly optimizes the fluid flow. Bawazeer and Alsoufi [2] examined convection for buoyancy-driven flow in a square cavity. They confirmed a strong standard for evaluating the precision of classical heat transfer behavior using a numerical benchmark dataset. Furthermore, Shoaib et al. [3] investigated the combined effects of thermal radiation and convection on Newtonian fluid flow over a vertical sheet. Nazir et al. [4] investigated convection and nonlinear thermal radiation in thermal transport of a Casson nanofluid flow, and Jan et al. [5] studied convection in double diffusion of viscous fluid flow within a porous and non-uniform cylinder undergoing stretching and shrinking nonlinear effects. Similarly, Y. H. et al. [6] investigated the impact of temperature-dependent viscosity models on a convection couple-stress fluid-saturated porous medium, and the

Volume 1, Issue 4, 2025
https://doi.org/10.5281/zenodo.17987780

results showed that increasing the couple-stress parameter enhances flow stability. In addition, Khan et al. [7] investigated the free convection of an Ostwald-de Waele fluid with a heated strip at the bottom of a chamber with a shaped middle. Shafiq et al. [8] and Nalimi et al. [9] investigated the dynamics of magnetohydrodynamic (MHD) flow over a permeable plate, combining the effects of convection with nonlinear stratification on heat and mass transfer processes. Increasing solutal and thermal stratification parameters in this context diminishes the concentration and temperature fields. Milon et al. [10] investigated the generation of internal heat and free flow convection through magnetohydrodynamics on an inclined porous plate, finding that the fluid velocity decreases with increasing inclination angle.

Viscoelastic fluids exhibit both viscous and elastic properties and are suitable for modeling a wide range of fluids. Ali et al. [11] examined the impacts of injection and suction on the Couette flow within a viscoelastic dusty fluid over an oscillating porous plate in a rotating frame. The results showed that the nanoparticle enhances heat transfer, and viscoelasticity influences velocity distribution. Khan et al. [12] studied the flow of a viscoelastic fluid between inclined divergent and convergent channels. Additionally, Ravikumar et al. [13] investigated the relationship between magnetohydrodynamic and electrokinetic forces during peristaltic activity in a viscoelastic fluid of a rotating system, which is essential for developing biomedical microdevices. Furthermore, Benaissa et al. [14] investigated the boundary layer flow of a Jeffery fluid through a stretching cylinder in an electrically conducting system. Hanafy and Tlili [15] studied the thermo-diffusion effects on viscoelastic fluid flow in the presence of a stretched cylinder with enhanced heat and mass transfer, particularly for larger curvature parameters. Additionally, Villada et al. [16] provided a formulation and evaluation of viscoelastic surfactants to design water-based drilling nanofluids, incorporating silica nanomaterials into the fluids. Furthermore, Kubinski et al. [17] studied Boger fluids, which exhibit rate-independent shear viscosity and elasticity, using torsional rheometers to measure the properties of viscoelastic fluids, and applied the Oldroyd-B model. Soni et al. [18] studied the elastic deformation of Cattaneo-Christov heat flux, Newtonian heating, viscous dissipation, and porous medium. In addition, Chen et al. [19] investigated the viscosity and elasticity of the shear drilling fluid as it passes through a reservoir, with a focus on controlling filtration loss. Meanwhile, Martin-Martin et al. [20] studied the electro-orientation using silver nanowire polymer solutions to form a gel network.

Porous medium deformation influences fluid flow and heat transfer. [21,22] developed models accounting for its impact on flow behavior. Biot [23] pioneered the study of deformable porous media, introducing the concept of poroelasticity. Coussy [24] developed the theory of one-dimensional consolidation of soils. Bowen [25] combined poroelasticity and poroplasticity to describe the behavior of deformable porous media. Auriault [26] treated the solid and fluid phases as interacting continua, and Lewis and Schrefler [27] averaged the properties of the solid and liquid phases. [28,29] explained the Two-scale modeling of ionic transport in deformable homogenization in a fluid-saturated porous medium using a linked fluid-solid SPH technique to model flow through deformable porous media. Using a theoretical treatment, Vernerey [30] studied the mechanics of interfaces in deformable porous media. Comprehensive models that include viscoelasticity, internal heat generation, and medium deformation, as well as an examination of non-Newtonian fluid dynamics in deformable porous media, are still lacking in considerable numbers despite current research. The beauty of this research lies in its exploration of a complex fluid dynamics problem that integrates the effects of hydro-magnetism and variable properties. The study advances the field of fluid mechanics by addressing previously underexplored aspects of hydro-magnetic Jeffery fluids.

Volume 1, Issue 4, 2025
https://doi.org/10.5281/zenodo.17987780

II. METHODOLOGY

(a). Model

The steady flow and heat transfer in a deformable porous medium flow are considered in this work. Internal heat generation is assumed to occur due to chemical interactions of fluid particles within the vertical channel. Therefore, the flow-governing equations are the elastic equilibrium equation, the momentum conservation equation, and the energy equation.

The governing equations [31] assume these forms

$$\left.\begin{aligned} &\frac{d^2u}{dy^2}-(1-\phi)\frac{dp}{dx}+\delta v=0,\quad u(\pm1)=0\\ &\frac{1}{1+\lambda_1}\frac{d^2v}{dy^2}-\phi\frac{dp}{dx}-(\delta+M)v+\theta=0,\ v(\pm1)=0\\ &\left(1+\frac{4}{3}R\right)\frac{d^2\theta}{dy^2}+\frac{N}{1+\lambda_1}\left(\frac{dv}{dy}\right)^2+N\delta v^2+\kappa\theta=0,\ \theta(\pm1)=1 \end{aligned}\right\} \quad (1)$$

Where the following dimensionless parameters and variables have been used

$$\left.\begin{aligned} &y=\frac{Y}{h},x=\frac{X}{h},v=\frac{2\mu_a V}{\rho g\beta h(T_1-T_0)},u=\frac{\mu U}{\rho g\beta h^2(T_1-T_0)},\ p=\frac{P}{\rho g\beta h(T_1-T_0)},\\ &\frac{N}{\left(1+\frac{4R}{3}\right)}=\tau,M^2=\frac{\sigma B_0^2h^2}{2\mu_a},R=\frac{4\sigma^*T_1^3}{k^*},N=\frac{\left(\rho g\beta^2h^2\right)^2(T_1-T_0)}{2\mu_a k_0},\theta=\frac{T-T_0}{T_1-T_0},\delta=\frac{Kh}{2\mu_a}. \end{aligned}\right\} \quad (2)$$

Theorem 1: There exists a unique solution to the coupled boundary value problem (1)

Proof: The first step is to convert the system of boundary value problems to its equivalent initial value problem using the shooting method. In view of this, we set

$$u=X_1,\ u'=X_2,\ v=X_3,\ v'=X_4,\ \theta=X_5,\ \theta'=X_6 \quad (3)$$

Such that

Volume 1, Issue 4, 2025
https://doi.org/10.5281/zenodo.17987780

$$\begin{pmatrix} X_1' \\ X_2' \\ X_3' \\ X_4' \\ X_5' \\ X_6' \end{pmatrix} = \begin{pmatrix} X_2 \\ (1-\phi)\dfrac{dp}{dx} - \delta X_3 \\ X_4 \\ (1+\lambda_1)\left(\phi\dfrac{dp}{dx} + (\delta+M)X_3\right) \\ X_6 \\ -\tau\left(\dfrac{X_4^2}{1+\lambda_1} + \delta X_3^2\right) \end{pmatrix} = \begin{pmatrix} f_1(X_1,X_2,X_3,X_4,X_5,X_6) \\ f_2(X_1,X_2,X_3,X_4,X_5,X_6) \\ f_3(X_1,X_2,X_3,X_4,X_5,X_6) \\ f_4(X_1,X_2,X_3,X_4,X_5,X_6) \\ f_5(X_1,X_2,X_3,X_4,X_5,X_6) \\ f_6(X_1,X_2,X_3,X_4,X_5,X_6) \end{pmatrix} \tag{4}$$

Together with the conditions

$$\begin{aligned} &X_1(-1)=0, \qquad X_3(-1)=0, \qquad X_5(0)=1 \\ &X_1'(-1)=C_1, \qquad X_4(0)=C_2, \qquad X_6(0)=C_3 \end{aligned} \tag{5}$$

where $C_{1,2,3}$ Are the guess values required for the boundary conditions at y=1 to be satisfied, evidently, $f_i(X_j)$, with $i,j=1,2,3,4,5,6$ They are continuous around the initial points; hence, they are bounded on the interval, since there is no singularity. Next, we need to establish the uniqueness; in this way, we need

$$\left.\begin{aligned} &\frac{\partial f_1}{\partial X_1}=0, \quad \frac{\partial f_1}{\partial X_2}=1, \quad \frac{\partial f_1}{\partial X_3}=\frac{\partial f_1}{\partial X_4}=\frac{\partial f_1}{\partial X_5}=\frac{\partial f_1}{\partial X_6}=0 \\ &\frac{\partial f_2}{\partial X_1}=0=\frac{\partial f_2}{\partial X_2}, \quad \frac{\partial f_2}{\partial X_3}=-\delta, \frac{\partial f_2}{\partial X_4}=\frac{\partial f_2}{\partial X_5}=\frac{\partial f_2}{\partial X_6}=0 \\ &\frac{\partial f_3}{\partial X_1}=0=\frac{\partial f_3}{\partial X_2}=\frac{\partial f_3}{\partial X_3}, \frac{\partial f_3}{\partial X_4}=1, \quad \frac{\partial f_3}{\partial X_5}=\frac{\partial f_3}{\partial X_6}=0 \\ &\frac{\partial f_4}{\partial X_1}=0=\frac{\partial f_4}{\partial X_2}, \quad \frac{\partial f_4}{\partial X_3}=(\delta+M)(1+\lambda_1), \frac{\partial f_4}{\partial X_4}=\frac{\partial f_4}{\partial X_5}=\frac{\partial f_4}{\partial X_6}=0 \\ &\frac{\partial f_5}{\partial X_1}=0=\frac{\partial f_5}{\partial X_2}, \frac{\partial f_5}{\partial X_3}=\frac{\partial f_5}{\partial X_4}=\frac{\partial f_5}{\partial X_5}, \frac{\partial f_5}{\partial X_6}=1 \\ &\frac{\partial f_6}{\partial X_1}=0=\frac{\partial f_6}{\partial X_2}, \frac{\partial f_6}{\partial X_3}=-2\tau\delta|X_3|=n_1, \frac{\partial f_6}{\partial X_4}=-2\tau\delta|X_4|=n_2, \frac{\partial f_6}{\partial X_5}=\frac{\partial f_6}{\partial X_6}=0 \end{aligned}\right\} \tag{6}$$

It is easy to conclude that

$$\frac{\partial f_i}{\partial X_j} \le \lambda \text{ and } \max\{\lambda_{ij}\} < \infty \tag{7}$$

Therefore, the first-order system of equations satisfies the Lipschitz condition for the existence of a unique solution.

Volume 1, Issue 4, 2025
https://doi.org/10.5281/zenodo.17987780

Theorem 2: Suppose the condition in Theorem 1 is satisfied, that is $f_i\left(X_j\right), \frac{\partial f_i}{\partial X_j}$ They are both continuous on the interval. Then there exists a unique solution to the problem.

Proof: let $\left(u_1,u_2\right),\left(v_1,v_2\right),\left(\theta_1,\theta_2\right)$ Are there any two solutions satisfying?

$$\left.\begin{aligned}
&\frac{d^2u_1}{dy^2}-(1-\phi)\frac{dp}{dx}+\delta v_1=0,\quad u_1\left(\pm1\right)=0\\
&\frac{1}{1+\lambda_1}\frac{d^2v_1}{dy^2}-\phi\frac{dp}{dx}-\left(\delta+M\right)v_1+\theta_1=0,\ v_1\left(\pm1\right)=0\\
&\left(1+\frac{4}{3}R\right)\frac{d^2\theta_1}{dy^2}+\frac{N}{1+\lambda_1}\left(\frac{dv_1}{dy}\right)^2+N\delta v_1^2=0,\ \theta_1\left(\pm1\right)=1
\end{aligned}\right\} \tag{8}$$

and

$$\left.\begin{aligned}
&\frac{d^2u_2}{dy^2}-(1-\phi)\frac{dp}{dx}+\delta v_2=0,\quad u_2\left(\pm1\right)=0\\
&\frac{1}{1+\lambda_1}\frac{d^2v_2}{dy^2}-\phi\frac{dp}{dx}-\left(\delta+M\right)v_2+\theta_2=0,\ v_2\left(\pm1\right)=0\\
&\left(1+\frac{4}{3}R\right)\frac{d^2\theta_2}{dy^2}+\frac{N}{1+\lambda_1}\left(\frac{dv_2}{dy}\right)^2+N\delta v_2^2=0,\ \theta_2\left(\pm1\right)=1
\end{aligned}\right\} \tag{9}$$

then $u_1=u_2,\ v_1=v_2,\theta_1=\theta_2$

Theorem: (Weierstrass Polynomial Approximation) Suppose theorems 1 and 2 hold, then there exists a sequence of Polynomials $u^N\left(y\right),\ \theta^N\left(y\right),\phi^N\left(y\right)$ Such that the polynomial functions approximate the solutions. i.e $u\left(y\right)\approx u^N\left(y\right),\ \theta\left(y\right)\approx\theta^N\left(y\right),\phi\left(y\right)\approx\phi^N\left(y\right)$.

Proof: Method of Solution

Equations (7)-(9) can be readily obtained via the spectral collocation method by assuming an admissible solution of the Chebyshev polynomials form $\Phi_j\left(y\right)$ as a sum of $N+1$ in which

$$\begin{aligned}
u\left(y\right)&\approx u^N\left(y\right)=\sum_{j=0}^{N}a_j\Phi_j\left(y\right),\\
\theta\left(y\right)&\approx\theta^N\left(y\right)=\sum_{j=0}^{N}b_j\Phi_j\left(y\right),\\
\phi\left(y\right)&\approx\phi^N\left(y\right)=\sum_{j=0}^{N}c_j\Phi_j\left(y\right)
\end{aligned} \tag{11}$$

Volume 1, Issue 4, 2025
https://doi.org/10.5281/zenodo.17987780

Where the (a_j, b_j, c_j) are coefficients to be determined based on the specified boundary conditions in (10)

$$R_1 = 1 + \left(\left(1+\kappa\left(u_y^N\right)^{\gamma-1}\right)u_y^N\right)_y - \left(Ha^2 + \beta^2\left(1+\kappa\left(u_y^N\right)^{\gamma-1}\right)\right)u^N + Gr\left(\theta^N + \sigma_1\theta^{2N}\right) + Gc\left(\phi^N + \sigma_2\phi^{2N}\right)$$

$$R_2 = \theta_{yy}^N + \lambda\left\{\phi\left(1+\varepsilon\theta^N\right)^m e^{\frac{\theta^N}{1+\varepsilon\theta^N}} + \delta\left(1+\kappa\left(u_y^N\right)^{\gamma-1}\right)\left(u_y^N\right)^2 + \left(Ha^2 + \beta^2\left(1+\kappa\left(u_y^N\right)^{\gamma-1}\right)\right)u^{2N}\right\} \quad (10)$$

$$R_3 = \left(e^{\alpha\phi}\phi_y^N\right)_y - Kr\lambda\phi^N\left(1+\varepsilon\theta^N\right)^m e^{\frac{\theta^N}{1+\varepsilon\theta^N}}$$

together with

$$u^N(\pm 1) = 0,\ \theta^N(\pm 1) = \theta_W,\ \phi^N(\pm 1) = 1. \quad (11)$$

The residues are forced to zero at the Gauss-Lobato points to get a system of nonlinear algebraic equations at

$$R_1(y_j) = R_2(y_j) = R_3(y_j) = 0, \quad j = 0,1,2,...,N \quad (12)$$

where y_i are defined

$$y_j = \frac{1}{2}\left(1 - \cos\left(\frac{j\pi}{N}\right)\right), \qquad j = 0,1,2,...,N \quad (13)$$

To avoid computational complexity, nonlinear equations (11)-(17) are carefully coded in Wolfram Mathematica 11, and the symbolic results are validated using the NDSolve algorithm, as presented in the following sections, Tables 1-3.

(b). Tabular and graphical results for spectral numerical study of internal heat-generating magnetoconvective fluid flow through poro-elastic media

The numerical solutions as well as the graphical results are shown below.

Table 1: $Ny = 30; \delta = 1; H = 1; \phi = 0.6; G = -1; \lambda_1 = 0.2; R = 1; m = 1;$

I	u(y)-SCM	u(y)-Shooting-RK4	ABSOLUTE ERROR
-1	0	$8.01227331308435 \times 10^{-18}$	$8.01227331308435 \times 10^{-18}$
-0.75	0.1696135682939229	0.16961356969372607	$399803162271951 \times 10^{-9}$
-0.5	0.2999052978346891	0.2999053003390014	$2.504312313078571 \times 10^{-9}$
-0.25	0.3814937562922307	0.38149375924863543	$956404732135098 \times 10^{-9}$
0.0	0.4092355306507757	0.4092355332574184	$2.606642679481297 \times 10^{-9}$
0.25	0.38149375736179175,	0.38149375924863543	$1.886843681297989 \times 10^{-9}$
0.5	0.2999053007336416,	0.2999053003390014	$3.946401538890143 \times 10^{-10}$
0.75	0.16961357155964887	0.16961356969372607	$1.865922805155406 \times 10^{-9}$
1	$2.877176535493689 \times 10^{-9}$	$8.085663848046625 \times 10^{-18}$	$2.877176527408025 \times 10^{-9}$

Volume 1, Issue 4, 2025
https://doi.org/10.5281/zenodo.17987780

Table 2: $Ny = 30; \delta = 1; H = 1; \phi = 0.6; G = -1; \lambda_1 = 0.2; R = 1; m = 1;$

Y	v(y)-SCM	v(y)- Shooting-RK4	ABSOLUTE ERROR
-1	0.	$1.629822429586848 \times 10^{-17}$	$1.462988459105453 \times 10^{-17}$
-0.75	0.23643919190180493	0.23643920645976688	$1.455796197480374 \times 10^{-8}$
-0.5	0.38479857099742854	0.3847985813316363	$1.033420793383754 \times 10^{-8}$
-0.25	0.4661356148423633	0.46613562163673067	$6.794367568563331 \times 10^{-9}$
0.0	0.4920208214582225	0.49202082586110873	$4.402886666365901 \times 10^{-9}$
0.25	0.4661356190805664	0.46613562163673067	$2.556165001887933 \times 10^{-9}$
0.5	0.3847985790324737	0.3847985813316363	$2.299163637253798 \times 10^{-9}$
0.75	0.236439207972135	0.23643920645976688	$1.512366565314948 \times 10^{-9}$
1	$1.33350846402352 \times 10^{-8}$	$1.487248760119362 \times 10^{-17}$	$1.33350823684545 \times 10^{-8}$

Table 3: $Ny = 30; \delta = 1; H = 1; \phi = 0.6; G = -1; \lambda_1 = 0.2; R = 1; m = 1;$

Y	Θ (y)-SCM	Θ (y)- Shooting-RK4	ABSOLUTE ERROR
-1	1.	1.0000000000000002	$2.220446049250313 \times 10^{-16}$
-0.75	1.0339005019742964	1.0339005128831338	$1.090883716692303 \times 10^{-8}$
-0.5	1.0528514706242837	1.0528514760594918	$5.435208061399521 \times 10^{-9}$
-0.25	1.0630217945308327	1.0630217967228472	$2.192014569857292 \times 10^{-9}$
0.0	1.0662875237975988	1.0662875289090126	$5.111413514669039 \times 10^{-9}$
0.25	1.0630217897436456	1.0630217967228472	$6.979201438994664 \times 10^{-9}$
0.5	1.0528514400159823	1.0528514760594918	$3.604350951036394 \times 10^{-8}$
0.75	1.0339004468331425	1.0339005128831338	$6.604999103210218 \times 10^{-8}$
1	0.9999999040360079	1.0000000000000002	$9.596399219713447 \times 10^{-8}$

Table 4: $Ny = 30; \delta = 1; H = 1; \phi = 0.6; G = -1; \lambda_1 = 0.2; R = 1; m = 1;$

Y	u (y)-SQLM	u (y)- Shooting-RK4	ABSOLUTE ERROR
0	0.409235533256931	0.4092355332574184	$4.873879078104437 \times 10^{-13}$
0.1	0.404778840588483	0.40477884291462063	$2.326137615860091 \times 10^{-9}$
0.2	0.391449858196354	0.3914498602689724	$2.072618410231541 \times 10^{-9}$
0.3	0.369372717082718	0.36937277597898843	$5.889627041621992 \times 10^{-8}$
0.4	0.338757626351711	0.33875768085692787	$5.450521683991738 \times 10^{-8}$
0.5	0.299905300338649	0.2999053003390014	$3.524402991672559 \times 10^{-13}$
0.6	0.253213702036002	0.25321377316787763	$7.113187561191836 \times 10^{-8}$
0.7	0.199187541813046	0.19918762605846557	$8.424541958484966 \times 10^{-8}$
0.8	0.138449136203938	0.138449141085021	$4.881082982244322 \times 10^{-9}$
0.9	0.071752353590178	0.07175235809515387	$4.50497587844989 \times 10^{-9}$
1.0	$-4.821663901477535 \times 10^{-15}$	$8.085663848046625 \times 10^{-18}$	$4.829749565325582 \times 10^{-15}$

Volume 1, Issue 4, 2025
https://doi.org/10.5281/zenodo.17987780

Table 5: $\mathrm{Ny} = 30; \delta = 1; H = 1; \phi = 0.6; G = -1; \lambda_1 = 0.2; R = 1; m = 1;$

Y	v (y)-SQLM	v (y)- Shooting-RK4	ABSOLUTE ERROR
0	0.49202082585997	0.49202082586110873	$1.138755756358023 \times 10^{-12}$
0.1	0.487919681716172	0.48791967648689993	$5.229272070916835 \times 10^{-9}$
0.2	0.475523859673885	0.4755238550201703	$4.65371469138276 \times 10^{-9},$
0.3	0.454554240908597	0.45455410827515325	$1.326334437279364 \times 10^{-7}$
0.4	0.424538007969754	0.42453788519490765	$1.227748463450417 \times 10^{-7}$
0.5	0.384798581330831	0.3847985813316363	$8.053002709118573 \times 10^{-13}$
0.6	0.334440527642153	0.33444036885219514	$1.587899578492368 \times 10^{-7}$
0.7	0.272328715385062	0.27232852818285236	$1.87202209622761 \times 10^{-7}$
0.8	0.197065228326544	0.1970652178929411	$1.043360289831873 \times 10^{-8}$
0.9	0.106960690152806	0.10696068038929912,	$9.76350687798 \times 10^{-9}$
1.0	$-9.765920711002352 \times 10^{-13}$	$1.487248760119362 \times 10^{-17}$	$9.766069435878363 \times 10^{-13}$

Table 6: $\mathrm{Ny} = 30; \delta = 1; H = 1; \phi = 0.6; G = -1; \lambda_1 = 0.2; R = 1; m = 1;$

Y	Θ (y)-SQLM	Θ (y)- Shooting-RK4	ABSOLUTE ERROR
0	1.066287528908974	1.0662875289090126	$3.863576125695545 \times 10^{-14}$
0.1	1.065768213396178	1.0657682129138761	$4.823019761346359 \times 10^{-10}$
0.2	1.064203149333608	1.0642031492696786	$6.392930629317561 \times 10^{-11}$
0.3	1.061568318963338	1.0615682932420807	$2.572125734623398 \times 10^{-8}$
0.4	1.057814314195811	1.0578142855452053,	$2.865060566570321 \times 10^{-8}$
0.5	1.052851476059487	1.0528514760594918	$4.884981308350689 \times 10^{-15}$
0.6	1.04652685599369	1.0465267616092888	$9.438440118358926 \times 10^{-8}$
0.7	1.038589938152717	1.0385898096924673	$1.284602497708675 \times 10^{-7}$
0.8	1.028645211531815	1.0286451981233322	$1.340848276853989 \times 10^{-8}$
0.9	1.016085681185261	1.0160856707147763	$1.047048470148581 \times 10^{-8}$
1.0	0.999999999999989	1.0000000000000002	$1.121325254871408 \times 10^{-14}$

Table 7: $\mathrm{Ny} = 30; \delta = 1; H = 1; \phi = 0.6; G = -1; \lambda_1 = 0.2; R = 1; m = 1;$

Y	u (y)-SQLM	u (y)- SCCM	ABSOLUTE ERROR
0	0.409235533256931	0.4092355306455976	$2.611333427271489 \times 10^{-9}$
0.1	0.404778840588483	0.4047788404661123	$1.223707246644778 \times 10^{-10}$
0.2	0.391449858196354	0.39140.39144985801071897,	$1.85635007365903 \times 10^{-10}$
0.3	0.369372717082718	0.369372773947350464698602689724	$5.686463244725104 \times 10^{-8}$
0.4	0.338757626351711	0.3387576790615619	$5.27098508729118 \times 10^{-8}$
0.5	0.299905300338649	0.29990529902725216	$1.311396824466015 \times 10^{-9}$
0.6	0.253213702036002	0.25321377237487797	$7.033887594598554 \times 10^{-8}$
0.7	0.199187541813046	0.1991876258188105	$8.400576451128572 \times 10^{-8}$
0.8	0.138449136203938	0.138449141422932	$, 5.218994181266368 \times 10^{-9}$

Volume 1, Issue 4, 2025
https://doi.org/10.5281/zenodo.17987780

0.9	0.071752353590178	0.07175235882095063	$5.23077263447913 \times 10^{-9}$
1.0	$-4.821663901477535 \times 10^{-15}$	$8.085663848046625 \times 10^{-18}$	$9.566542899179229 \times 10^{-10}$

Table 8: $\mathrm{Ny} = 30; \delta = 1; H = 1; \phi = 0.6; G = -1; \lambda_1 = 0.2; R = 1; m = 1;$

Y	v (y)-SQLM	v (y)- SCCM	ABSOLUTE ERROR
0	0.409235533256931	0.4092355332574184	$4.390997121461737 \times 10^{-9}$
0.1	0.404778840588483	0.40477884291462063	$8.76322159282239 \times 10^{-9}$
0.2	0.391449858196354	0.3914498602689724	$7.293694315180233 \times 10^{-9}$
0.3	0.369372717082718	0.36937277597898843	$1.344151012161454 \times 10^{-7}$
0.4	0.338757626351711	0.33875768085692787	$1.23665776674553 \times 10^{-7}$
0.5	0.299905300338649	0.2999053003390014	$6.795036755491424 \times 10^{-11}$
0.6	0.253213702036002	0.25321377316787763	$1.57859909588609 \times 10^{-7}$
0.7	0.199187541813046	0.19918762605846557	$1.85084136739011 \times 10^{-7}$
0.8	0.138449136203938	0.138449141085021	$6.370570765357186 \times 10^{-9}$
0.9	0.071752353590178	0.07175235809515387	$3.240017906747106 \times 10^{-9}$
1.0	$-4.821663901477535 \times 10^{-15}$	$8.085663848046625 \times 10^{-18}$	$1.001626639767299 \times 10^{-8}$

Table 9: $\mathrm{Ny} = 30; \delta = 1; H = 1; \phi = 0.6; G = -1; \lambda_1 = 0.2; R = 1; m = 1;$

Y	θ(y)-SQLM	θ (y)- SCCM	ABSOLUTE ERROR
0	0.409235533256931	0.4092355332574184	$5.03298114296058 \times 10^{-9}$
0.1	0.404778840588483	0.40477884291462063	$5.119088930527482 \times 10^{-9}$
0.2	0.391449858196354	0.3914498602689724	$4.269768760778447 \times 10^{-9}$
0.3	0.369372717082718	0.36937277597898843	$2.953535549465869 \times 10^{-8}$
0.4	0.338757626351711	0.33875768085692787	$3.212274091168865 \times 10^{-8}$
0.5	0.299905300338649	0.2999053003390014	$7.434007409656829 \times 10^{-9}$
0.6	0.253213702036002	0.25321377316787763	$1.086123517790582 \times 10^{-7}$
0.7	0.199187541813046	0.19918762605846557	$1.529545590184255 \times 10^{-7}$
0.8	0.138449136203938	0.138449141085021	$5.30024995004652 \times 10^{-8}$
0.9	0.071752353590178	0.07175235809515387	$6.441063593598528 \times 10^{-8}$
1.0	$-4.821663901477535 \times 10^{-15}$	$8.085663848046625 \times 10^{-18}$	$6.368073557361242 \times 10^{-8}$

Volume 1, Issue 4, 2025
https://doi.org/10.5281/zenodo.17987780

Table 10: Convergence of SCCM when $\delta = 1; H = 1; \kappa = 0.6; G = -1; \lambda_1 = 0.2; R = 1; m = 1;$

Np	U	v	Θ
5	0.2997447935041984	0.3852450995917389	1.0536862034834673
10	0.29990530058383363	0.38479858000289674	1.0528514838665468
15	0.29990530033897844	0.3847985813315716	1.0528514760591237
20	0.2999053003390013	0.3847985813316363	1.0528514760594918
25	0.29990530033900137	0.3847985813316363	1.0528514760594918
30	0.2999053003390014	0.3847985813316363	1.0528514760594918
35	0.2999053003390013	0.3847985813316362	1.0528514760594918
40	0.2999053003390013	0.3847985813316362	1.0528514760594918

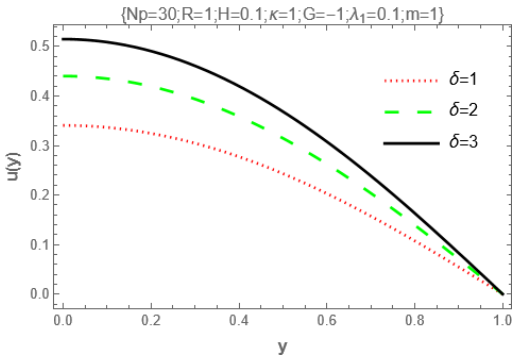

Figure 1: Effect of Porous Permeability on Solid Displacement.

Figure 1 shows the effect of porous permeability on the solid displacement within the flow channel. From the results, increasing values of the porous permeability parameter lead to an increase in solid displacement due to a reduction in fluid viscosity within the flow passage. Since $\delta = D\left(\frac{1}{Da}\right)$ Then, as the porous permeability parameter increases, the flow velocity decreases. In fact, flow increases as flow barriers decrease.

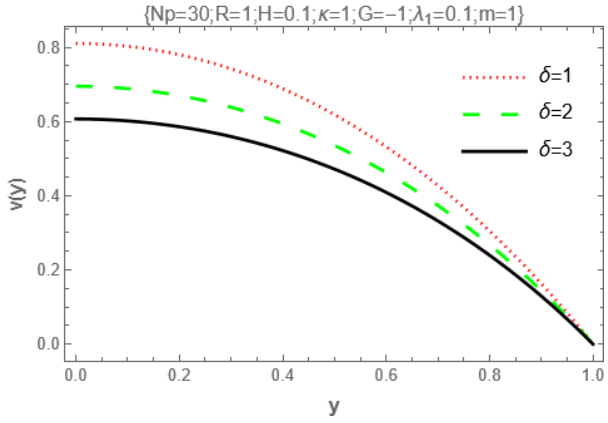

Figure 2: Effect of Porous Permeability on Flow Velocity

Volume 1, Issue 4, 2025
https://doi.org/10.5281/zenodo.17987780

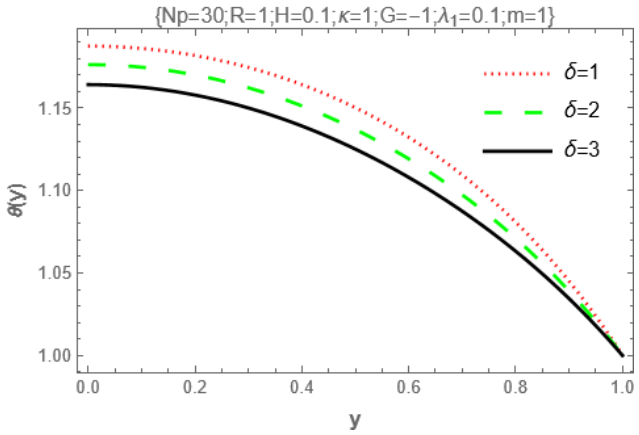

Figure 3: Effect of Porous Permeability on Fluid Temperature

Similarly, as porous permeability increases, heat retention is high within the flow channel, as seen in the plot.

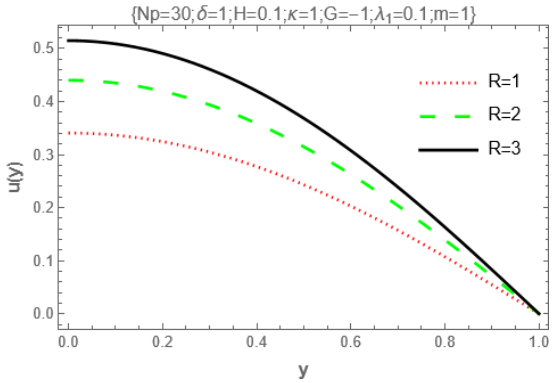

Figure 4: Effect of Thermal Radiation on Solid Displacement

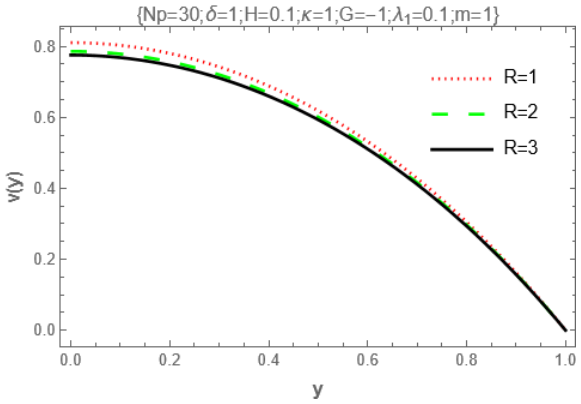

Figure 5: Effect of Thermal Radiation on Flow Velocity

Volume 1, Issue 4, 2025
https://doi.org/10.5281/zenodo.17987780

The effect of thermal radiation is presented on solid displacement, flow velocity, and fluid temperature, respectively, in figures (4) – (6). The results show that as the thermal radiation parameter increases, solid displacement rises, while velocity and temperature decrease. The reason is that radiation reduces the total heat in a body, while viscosity absorbs radiation from the walls.

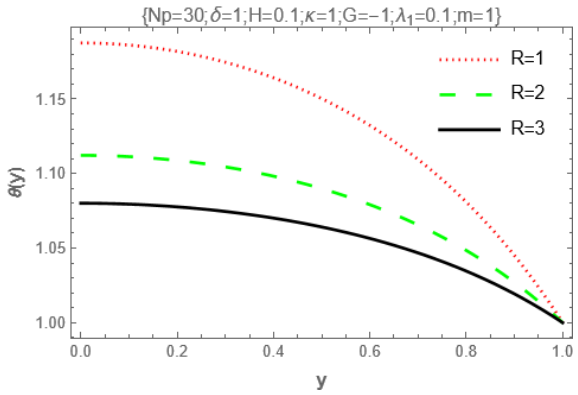

Figure 6: Effect of thermal radiation on fluid temperature

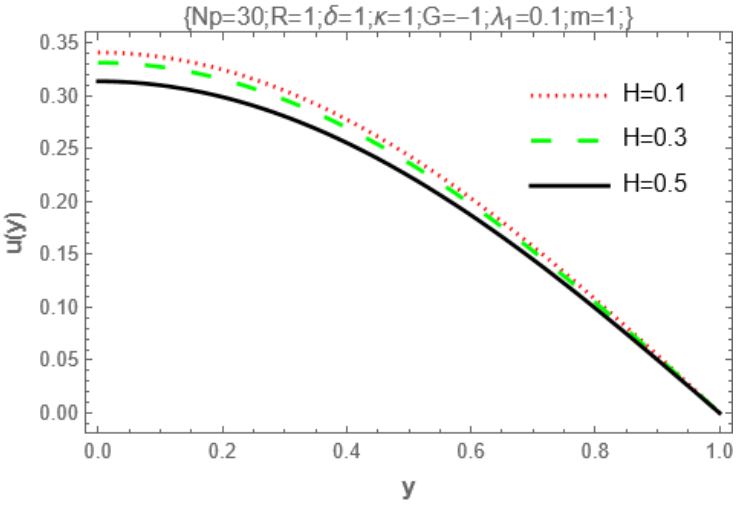

Figure 7: Effect of Hartman number on the solid displacement

The effect of the magnetic field on the convective flow is shown here in figures (7) – (8). From this graph, it is evident that the magnetic field intensity decreases the flow field due to the actions of Lorentz forces on the magnetic flow particles.

Volume 1, Issue 4, 2025
https://doi.org/10.5281/zenodo.17987780

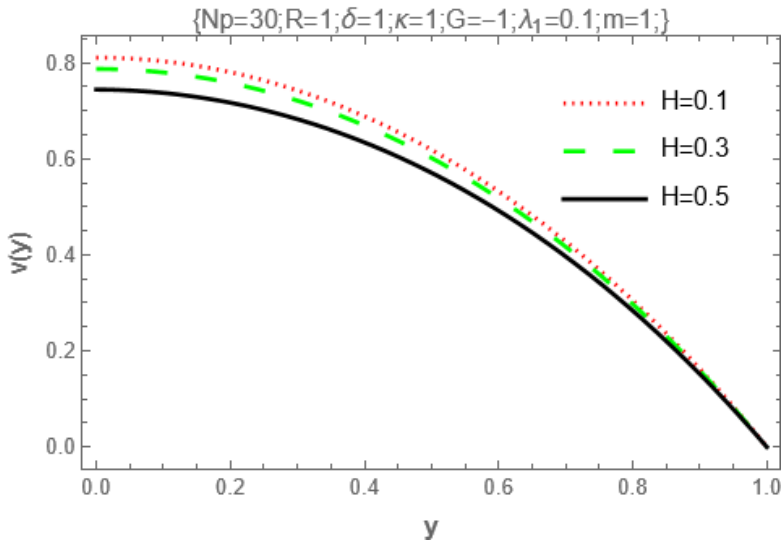

Figure 8: Effect of Hartman Number on Flow Velocity

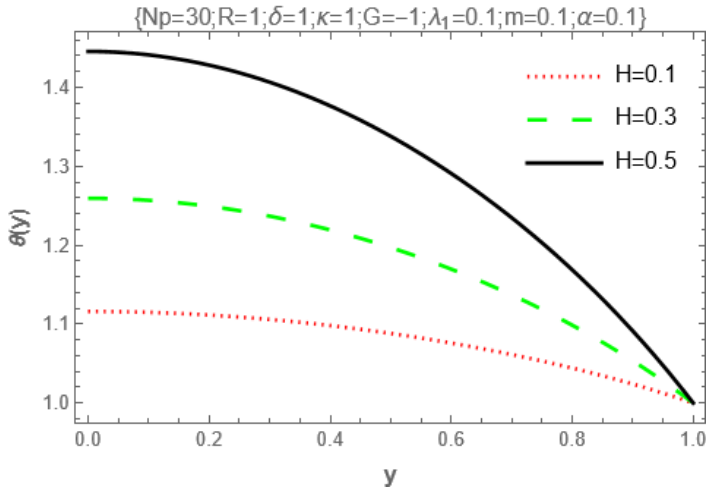

Figure 9: Effect of Hartman Number on Fluid Temperature

Volume 1, Issue 4, 2025
https://doi.org/10.5281/zenodo.17987780

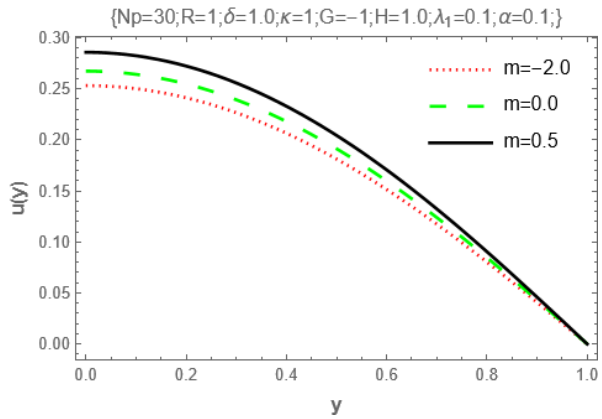

Figure 10: Effect of Kinetic Parameter on Solid Displacement

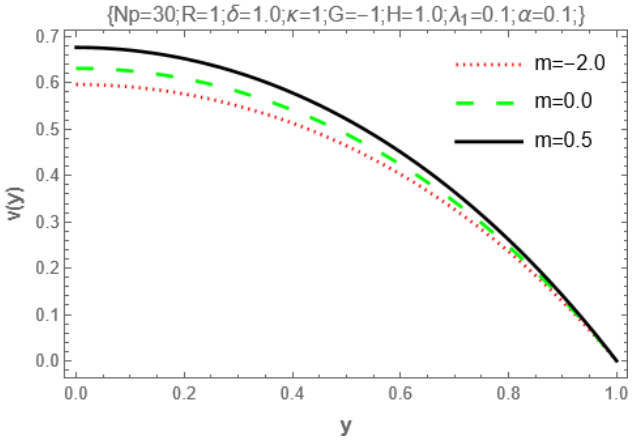

Figure 11: Effect of Kinetic Parameter on Fluid Velocity

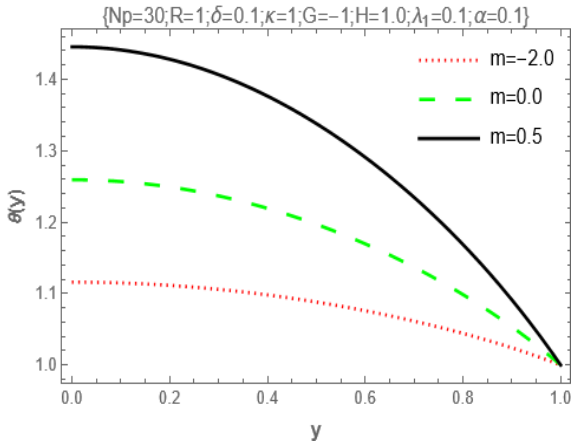

Figure 12: Effect of Kinetic Parameter on Fluid Temperature

Volume 1, Issue 4, 2025
https://doi.org/10.5281/zenodo.17987780

DISCUSSION OF RESULTS

The numerical investigation conducted in this paper gives valuable insights into the behavior of a radiative magneto-convective Jeffery fluid flowing through a deformable porous medium with internal heat generation. The comparison between the spectral methods (SCM, SQLM, and SCCM) and the Shooting Runge-Kutta (RK4) method demonstrates a strong agreement across all displacement, velocity, and temperature profiles. The consistently minor absolute errors observed in Tables 1–9 confirm the reliability and uniqueness of the proposed solution, in accordance with the earlier theorems established in the work. The results in Figures 1–3 highlight the importance of porous permeability on the overall behavior of the system. As permeability increases, it easily leads to increased displacement within the channel. This agrees with physical expectations, as reduced flow resistance promotes more effortless movement of both fluid and solid phases. Interestingly, while permeability increases solid displacement, the fluid velocity reduces. This indicates that the ease of deformation absorbs part of the driving force that would otherwise accelerate the fluid. However, temperature rises with increasing permeability due to reduced convective heat removal, allowing thermal energy to accumulate within the channel.

The effect of thermal radiation, as shown in Figures 4–6, exhibits distinct behavior across the three field variables. Solid displacement increases with increasing radiation intensity, suggesting that radiation enhances the thermal softening of the porous media. However, both velocity and temperature decrease under more substantial radiation effects. This outcome aligns with the physical understanding that radiation enhances heat loss from the system, thereby reducing the thermal energy available to drive fluid motion. The reduction in temperature also limits thermal expansion, further contributing to the observed decline in velocity. The effect of the magnetic field, represented by the Hartmann number in Figures 7–9, follows classical magnetohydrodynamic behavior. As the Hartmann number increases, Lorentz forces oppose fluid motion, resulting in a measurable decline in velocity. This suppression effect also influences the displacement field, resulting in a decrease in solid deformation. The temperature, however, shows varying sensitivity, with the trend indicating that the magnetic field stabilizes the thermal boundary layer by restricting fluid motion and reducing convective heat transport. The influence of the kinetic parameter, as illustrated in Figures 10–12, is that an increase in this parameter enhances displacement, velocity, and temperature simultaneously. This is expected because internal heat generation introduces additional thermal energy into the system, thereby raising the fluid temperature and reducing its viscosity. The resulting thermal expansion and lowered resistance allow the fluid to move more freely, which in turn increases the deformation of the porous structure. Overall, the discussion of results underscores the interplay between magnetic, radiative, and porous effects in controlling the flow behavior of a Jeffery fluid in a deformable porous medium. More importantly, the excellent match between all numerical schemes confirms that the spectral approach employed in this study is robust and accurate.

III. CONCLUSION

This study presents a comprehensive spectral numerical analysis of internal heat-generating magneto-convective Jeffery fluid flow through a poroelastic channel. By applying the shooting Runge-Kutta method in conjunction with Spectral Collocation and Spectral Quasi-Linearization methods, the work validates the existence and uniqueness of the solution to the coupled nonlinear boundary value problem. The research demonstrates that permeability, thermal radiation, magnetic fields, and kinetic heat generation have a great significant influence on displacement, velocity, and temperature fields. Porous permeability enhances solid displacement but suppresses velocity,

Volume 1, Issue 4, 2025
https://doi.org/10.5281/zenodo.17987780

while radiation reduces temperature and flow speed due to increased heat loss. The magnetic field consistently dampens fluid movement through Lorentz forces, whereas internal heat generation intensifies all field variables. In addition to uncovering the physical behavior of the system, the study confirms the reliability and convergence of spectral techniques for solving complex non-Newtonian, porous-medium fluid models. The strong agreement across numerical methods strengthens the credibility of the findings and positions spectral schemes as efficient alternatives to conventional solvers.

REFERENCES

[1] Sathyendar Sreepada, Surender Ontela (2025). Spectral analysis of nonlinear free convective flow of a Casson fluid in a non-Darcy porous medium with convective boundary condition. Following Materials 9, 101043

[2] Saleh A. Bawazeer, Mohammad S. Alsoufi. (2025). Natural convection in a square Cavity: Effects of Rayleigh and Prandtl numbers on heat transfer and flow patterns. Case Studies in Thermal Engineering 73, 106680

[3] Muhammad Shoaib, Shafaq Naz, Muhammad Asif Zahoor Raja, Khadeeja Arshad, Iftikhar Ahmad, Kottakkaran Sooppy Nisa (2025). Numerical treatment for nonlinear mixed convection and thermal radiative Newtonian fluid flow system. Journal of Radiation Research and Applied Sciences, 18, 101675

[4] Faisal Nazir, Jawad Ahmed, Thabet Abdeljawad, Ali Alshamrani, Khadijah M. Abualnaja, Mohamed Abdelghany Elkotb (2025). Analysis of thermal and solutal transport in Casson nanofluid flow around a rotating cylinder subject to mixed convection and radiation. Case Studies in Thermal Engineering, 74, 106663

[5] Nadeem Jan, Dil Nawaz Khan Marwat, Ali Althobaiti, Ahmed Shafee, Asfandyar Khan, Fazal Ghani (2026). Double diffusive convection in flow along a heated and non-uniform cylinder with nonlinear kinematics. Kuwait Journal of Science 53, 100489

[6] Gangadharaiah Y H, Vijaya Kumar, Manjunatha N, Nagarathnamma H, Maryam Ali Alghafli, Irshad Ayoob, Nabil Mlaiki (2025). Convective stability in porous structures for energy and biosensing applications using viscosity-driven flow control and couple-stress fluid. Case Studies in Thermal Engineering, 75, 107189

[7] Md. Jubair Khan, Md. Fazla Rabbi Jim Islam, Sumon Saha (2024). The free convective flow of Ostwald-de Waele fluid in a Π-shaped cavity with a heated strip and lateral wall cooling. Results in Engineering 24 103167

[8] Anum Shafiq, Tabassum Naz Sindhu, Muhammad Ahmad Iqbal, Tahani A. Abushal. (2025). Nonlinear squeezing flow of stratified fluids: A comprehensive study on convective conditions and probable errors. International Journal of Thermofluids 28, 101290.

[9] Rajendran Nalini, Athimoolam Meena, Lakshmanan Rajendran, Mohammad Izadii (2025). A nonlinear mathematical analysis of nanoparticles' velocity, temperature, and concentration in magnetohydrodynamic convective flow. Partial Differential Equations in Applied Mathematics. 14, 101193

[10] Mahamudul Hassan Milon, Md Hasanuzzaman, Ashish Barmon, Md. Asaduzzaman (2025). Impact of internal heat production and absorption on an unstable MHD free convective flow through an inclined porous plate. International Journal of Thermofluidsate. 29 101403.

[11] Srivastava, V. P. (2017). Viscoelastic fluid flows through porous media with internal heat generation. Journal of Porous Media, 20(10), 845-858. doi: 10.1615/JPorMedia.v20.i10.10.

[12] Park, H. M. & Lee, S. J. (2019). Viscoelastic flow through porous media: Effects of Darcy-Forchheimer drag and internal heat generation. Journal of Non-Newtonian Fluid Mechanics, 265, 109-121. doi: 10.1016/j.jnnfm.2019.02.004.

https://doi.org/10.5281/zenodo.17987780

[13] Makinde, O. D. & Ogulu, A. (2008). The effect of thermal radiation on the heat and mass transfer flow of a variable viscosity fluid past a vertical porous plate permeated by a transverse magnetic field. Chemical Engineering Communications. 195(12), 1575-1584.https://doi.org/10.1080/00986440802115549.
[14] M.M. Bhatti, A. Zeeshan, N. Ijaz, O. Anwar Bég, A. Kadir (2017). Mathematical modeling of nonlinear thermal radiation effects on EMHD peristaltic pumping of viscoelastic dusty fluid through a porous medium duct. Engineering Science and Technology, an International Journal 20 1129 – 1139.
[15] Amin Samimi Behbahan, As'ad Alizadeh , Meysam Mahmoudi , Mahmoud Shamsborhan , Tariq . Al-Musawi, Pooya Pasha. (2023). A new Adomian decomposition technique for a thermal analysis of forced non-Newtonian magnetic Reiner-Rivlin viscoelastic fluid flow. Alexandria Engineering Journal 80 48 -57
[16] Hongbo Chen, Ergun Kuru & Ke Hu (2024). A comparative study of the water-based drilling fluid viscoelasticity versus shear viscosity effects on the filtration loss control. 241 213117.
[17] Barnes, H. A., Hutton, J. F., & Walters, K. (1989). An Introduction to Rheology. Elsevier Science
[18] White, C. M., and Mungal M. G. (2008). Mechanics and Prediction of turbulent drag reduction with polymer additives. Annual Review of Fluid Mechanics. 40. 235-256
[19] Groisman, A., & Steinberg, V. (2000). Elastic turbulence in a polymer solution flow. Nature, 405 (6782), 53-55
[20] Rao, M. A. (2014). Rheology of fluid, semisolid, and solid foods: Principles and Applications. Springer.
[21] Auriault J. L. & Lewandowska, J. (2019). Deformable porous media: Theory and applications. Journal of Porous Media, 22(1), 1-13. doi:10.1615/JPorMedia.v22.i1.10
[22] Yortsos, Y. C. (2017). Deformable porous media: Dynamics and transport. Transport in Porous Media, 116(2), 251-265. doi: 10.1007/s11242-017-0851-4
[23] Biot, M. A. (1941). General theory of three-dimensional consolidation. Journal of Applied Physics, 12(2), 155-164.
[24] Coussy, O. (2004). Poromechanics. Wiley.
[25] Bowen, R. M. (1980). Incompressible porous media models by use of the theory of mixtures. International Journal of Engineering Science, 18(9), 1129-1148.
[26] Auriault, J. L. (1991). Heterogeneous medium. Isobar.
[27] Lewis, R. W., & Schrefler, B. A. (1998). The finite element method in the static and dynamic deformation and consolidation of porous media. Wiley.
[28] Ha H. Bui, Giang D. Nguyen (2017). A coupled fluid-solid SPH approach to modeling flow through deformable porous media. International Journal of Solids and Structures 125 244-264
[29] Jana Turjanicová, Eduard Rohan, Vladimír Lukeš (2019). Homogenization-based two-scale modeling of ionic transport in fluid-saturated deformable porous media. Computers and Mathematics with Applications 78 3211 – 3235.
[30] Franck J. Vernerey (2011). A theoretical treatment on the mechanics of interfaces in deformable porous media, International Journal of Solids and Structures 48 3129–3141
[31] Mallikarjuna, B., Srinivas, J., Gopi Krishna, G., Anwar Beg, O., and Kadir, A. (2021): Spectral Numerical study of Entropy Generation in Magneto-Convective Viscoelastic Biofluid flow through poro-elastic media with thermal radiation and buoyancy effects